IOP Conf. Series: Materials Science and Engineering **373** (2018) 012021 doi:10.1088/1757-899X/373/1/012021

Heat treatment condition of EN AW-7075 influencing the anodic oxidation process and coating properties

R Morgenstern*, I Scharf and T Lampke

Institute of Materials Science and Engineering, Chemnitz University of Technology, 09125 Chemnitz, Germany,

* e-mail: roy.morgenstern@mb.tu-chemnitz.de

Abstract. The age-hardenable aluminium alloy EN AW-7075 exhibits outstanding specific mechanical properties and therefore offers a high potential for lightweight construction. Anodising in aqueous oxalic acid solutions is suitable to produce a protective oxide ceramic conversion layer on this alloy. This study examines the influence of the precipitation state of the substrate alloy on microstructure and properties of anodic oxide layers. Therefore, EN AW-7075 sheets in the heat treatment conditions T4, T6 and T73 were anodized in 0.8 M oxalic acid solution at constant voltage. The current efficiency was determined on the basis of the electrical charge quantity, coating thickness and coating mass. Instrumented indentation tests were applied in order to evaluate the coating hardness. The microstructure of the anodic oxide layer was illustrated using field emission electron microscopy. It was shown that the current efficiency strongly depends on the heat treatment condition.

1. Introduction

Due to the highest mechanical strength among aluminum alloys, the 7xxx series are widely applied for lightweight constructions in automotive and aerospace applications. However, the low hardness and high adhesion tendency of aluminum alloys limit their applicability under tribological load. This restriction can be overcome by the generation of hard alumina conversion coatings using the anodic oxidation process [1]. Industrial anodizing processes are typically conducted in sulfuric acid electrolytes, because of the low process costs. Conversion coatings with a high maximum thickness, high hardness and a low hardness decline across the coating thickness can be obtained by reducing the bath temperature below 5 °C. This is due to the reduced chemical dissolution of the pore walls and hence the lower conicity of the pore walls. Unfortunately, additional energy and equipment costs arise from the electrolyte cooling and the increasing process voltage. Accepting higher process voltages, anodic aluminum oxide (AAO) coatings with a comparably high hardness and low hardness gradient can be obtained without extensive electrolyte cooling from oxalic acid electrolytes at room temperature, alternatively. Currently, efforts are made in order to generate wear resistant anodic oxide coatings only at tribologically stressed functional surfaces of components. This enables further savings in energy and chemicals and dimensional tolerances of other component surfaces are not affected. This can be realized, inter alia, using sealed electrochemical cells, e.g. capillary cells [2, 3] or open systems, e.g. continuous electrolyte jet anodizing [4]. Especially for the latter processes, oxalic acid electrolytes might be more suitable due to less corrosion of the plant equipment compared with sulfuric acid electrolytes.

As anodizing operates by the conversion of the substrate material, the coating properties are not only determined by the process characteristics (e.g. electrolyte, temperature, electrical parameters) but also by the chemical composition and the microstructure of the substrate alloy. Because of the less negative enthalpy of oxide formation compared with Al, the main alloying element of 7xxx alloys Zn enriches at the substrate-coating interface during anodic oxidation, while Al is preferably oxidized. Regarding model alloys containing 0.2 to 0.9 at% (0.5 to 2.2 wt%) Zn, the authors Zhou et al. observed a Zn enriched zone with a Zn concentration of at least 7.8 at% (17 wt%) and a thickness of up to 10 nm [5]. Apart from a higher Zn content of 5.5 wt%, alloy EN AW-7075 contains up to 2.9 wt% Mg, up to 2 wt% Cu and small amounts of Fe, Si, Mn, Cr und Ti. Similar to Zn, the elements Cu, Cr and Fe are enriched at substrate-alloy interface during anodizing, as well. However, being semi-conductors, the oxides of these elements allow electronic conduction, thus enabling oxygen generation at the anode. With proceeding oxide growth, the emerging gas bubbles leave small voids along the pore channels [6]. Consequences are an increased coating porosity and a reduced current efficiency of oxide formation. Investigations at different heat treatment conditions of the alloy EN AW-2024 (AlCu4Mg1) showed that the oxide formation is less negatively affected, if the element Cu is not homogeneously dispersed in the Al solid solution (Alss) or in the form of atomic clusters but bound in Al_2CuMg precipitates as they are rapidly dissolved during the anodizing process [7].

It might be reasonably assumed, that the conversion and dissolution behavior of intermetallic phases determines the anodizing behavior of alloy EN AW-7075 as the elements Fe, Mn and Cr are almost insoluble in the Alss, even at elevated temperatures. They already form primary precipitates during the solidification process and may also bind Cu atoms. Mukhopadhyay et al. observed $Al_{12}(FeMn)_3Si$ precipitates containing a small amount of Cu and Cr with a size of up to 12 µm in alloy EN AW-7075 with commercial purity [8]. These coarse precipitates are not completely dissolved during anodizing in a sulfuric acid electrolyte and locally impede the oxide growth. This results in an increasing process voltage [8]. In contrast, the Al_7Cu_2Fe phase, which dissolves during anodizing without impeding the process significantly, was observed in a model alloy containing smaller amounts of the impurities Si, Mn and Fe [8]. This is confirmed by Veys-Renaux et al. who observed the dissolution of the Al_7Cu_2Fe phase during anodizing of EN AW-7175 (same alloy composition as EN AW-7075, lower impurity content) in a sulphuric acid electrolyte [9]. Moreover, the authors observed that the strengthening precipitates $MgZn_2$, AlCuMg and Al_2CuMg are also dissolved during anodizing leaving voids with corresponding sizes between 100 and 200 nm within the oxide conversion coating [9]. Growth rate and current efficiency are similar for the anodizing of alloy EN AW-7175 and commercially pure aluminum (EN AW-1050, Al99.5) and significantly larger compared with alloy EN AW-2618 [9]. Although, the heat treatment conditions of EN AW-7175 and EN AW-2618 are not mentioned explicitly, some conclusions can be drawn on the basis of the microstructural descriptions. Presumably, alloy EN AW-7175 was used in an overaged condition because the strengthening phases were no longer present as Guinier-Preston (GP) zones, but already as stoichiometric phases. On the contrary, no strengthening phases could be detected for the EN AW-2618 alloy; thus a naturally aged condition (e.g. T3, T4) can be suggested. The results of Veys-Renaux et al. [9] broadly correspond with those of Morgenstern et al. [7] indicating that the properties of anodic oxide coatings are not only influenced by the alloy composition but also by the distribution of the alloying elements and therefore by the heat treatment state.

Up to the present, the impact of the heat treatment condition of EN AW-7075 on the properties of anodic oxide coatings is not covered systematically. Furthermore, few knowledge is available on the dissolution and conversion behavior of precipitates in EN AW-7075 during anodizing in oxalic acid electrolytes. The current article strives to close these knowledge gaps and to explain the complex correlations between substrate microstructure (precipitates), process characteristics (e.g. current efficiency), coating microstructure (porosity) and coating properties (coating thickness and hardness). Furthermore, the article is focused on the industrially important conditions T6 (highest strength) and T73 (improved resistance against stress corrosion cracking). Additionally, the naturally aged state T4 is included as a reference state.

2. Materials and methods

Sheets of the aluminum alloy AlZn5.5MgCu (EN AW-7075, nominal composition in wt%: Si ≤ 0.4, Fe ≤ 0.5, Cu 1.2–2.0, Mn ≤ 0.3, Mg 2.1–2.9, Cr 0.18–0.28, Zn 5.1–6.1, Ti ≤ 0.2) with the dimensions of 100 x 25 x 1.5 mm³ were used as substrate material. All sheets were solution annealed (470 °C, 1 h) and quenched in water, followed by natural aging (room temperature, > 14 days, condition T4), peak aging (120 °C, 24 h, condition T6) and overaging (120 °C, 24 h and 160 °C, 30 h, condition T73) according to [10].

Three samples of each heat treatment condition were prepared for anodizing. Sample pretreatment included etching in 3 wt% NaOH solution (60 °C, 3 min) and pickling in 1:1 diluted nitric acid (room temperature, 30 s). The electrolyte for the anodic oxidation was comprised of 0.8 mol/l oxalic acid (supplied as oxalic acid dehydrate, Merck). The electrolyte temperature was 25 °C. All the used chemicals were of analytical grade. The anodizing voltage was linearly increases from 0 to 60 V within 30 s and afterwards kept constant at 60 V. The electrolyte was constantly stirred during the total anodizing duration of 15 min. The power supply was a pe1028 (Plating Electronic). The values of current and voltage were logged internally during the process with an acquisition rate of 1 sample per second. The electrical charge per area was calculated by the integration of the current density profile over the anodizing time. The coating thickness was measured by optical microscopy on the cross-sections of all samples.

The mass of all samples was determined before and after the dissolution of the conversion coating in chromic/phosphoric acid (35 ml/l phosphoric acid + 20 g/l chromium(VI)oxide) at 60 °C for 4 h with a X1003S balance (Mettler Toledo). Pretests showed that no measureable dissolution of the substrate alloy occurs during the exposition in chromic/phosphoric acid, therefore, the mass difference equals to the coating mass. The porosity p of the coatings was estimated by the following formula using the coating mass m, the surface area A, the coating thickness s and the density of alumina ρ (3.95 g/cm^3):

$$p = 1 - \frac{m}{A*s*\rho} \tag{1}$$

The current efficiency η was determined by dividing the coating mass m by the theoretical mass m_{th}. The theoretical mass m_{th} was calculated according to the Faraday´s law using the electrical charge Q, the molecular mass M of Al_2O_3 (101,96 g/mol), the number of electrons involved in the generation of one Al_2O_3 molecule (u = 6) and the Faraday constant F (96485,33289 As/mol):

$$m_{th} = \frac{Q*M}{u*F} \tag{2}$$

Metallographic cross-sections were prepared by diamond grinding accomplished by a finish using a silica oxide polishing suspension. The microstructure was investigated by field emission scanning electron microscopy (FE-SEM, Zeiss, NEON40EsB). Both secondary electron (SE, topography contrast) and backscattered electron (QBSD, element contrast) detectors were applied. Hardness profiles of the AAO cross-sections were obtained from instrumented indentation tests at the cross sections of the coatings with a Berkovich indenter (Asmec Unat) by placing the indents at different locations and measuring the distances of the indents from the substrate surface via optical microscopy. A load of 5 mN was applied (load time 10 s, hold time 5 s, unload time 4 s).

3. Results and discussion

3.1. Current efficiency

Typical current density profiles for the anodic oxidation of different heat-treatment conditions of EN AW-7075 are shown in figure 1. During the first seconds, the current rises steeply with the increasing anodic potential. After 30 s, the constant potential of 60 V is reached and soon afterwards, a continuous and dense alumina barrier layer evolved. Because of the presence of the electrically insulating barrier layer, the anodic current is reduced to a minimum after about 50 to 100 s. With the concentration of the current flow at weaknesses of the barrier layer, the anodic dissolution becomes localized and pores evolve. The steady growth of the coating thickness is accompanied by a slight increase of the anodic current. It can be seen from figure 1 that the current density profile for the T4 condition runs at a slightly higher level compared with the T6 condition, whereas a significantly lower current level can be observed for the T7 condition. This observation is quantitatively displayed by the electrical charge density σ_q in table 1. Accordingly, the electrical charge quantity σ_q decreases with increasing intensity of the aging treatment from the condition T4 to T7 by about 30 %. Exactly the same proportional decline can be observed for the coating mass per area (referred to as specific mass). Consequently, the current efficiency, i.e. the amount of oxide generated from a certain amount of electrical charge, is constant. In relation to the maximum possible coating mass according to the Faradays law, the current efficiency amounts to about 46 % for all heat treatment conditions. Furthermore, the coating thickness also decreases by about 30 %. As the coating thickness is proportional to the specific coating mass, a constant overall coating density can be assumed. Considering the density of alumina, a coating porosity of about 43 % applies to all heat treatment conditions. Summarizing the above, it can be stated that the aging condition only influences the anodic charge quantity. Coating mass and coating thickness change accordingly and mass-related properties, e.g. current efficiency and porosity stay constant.

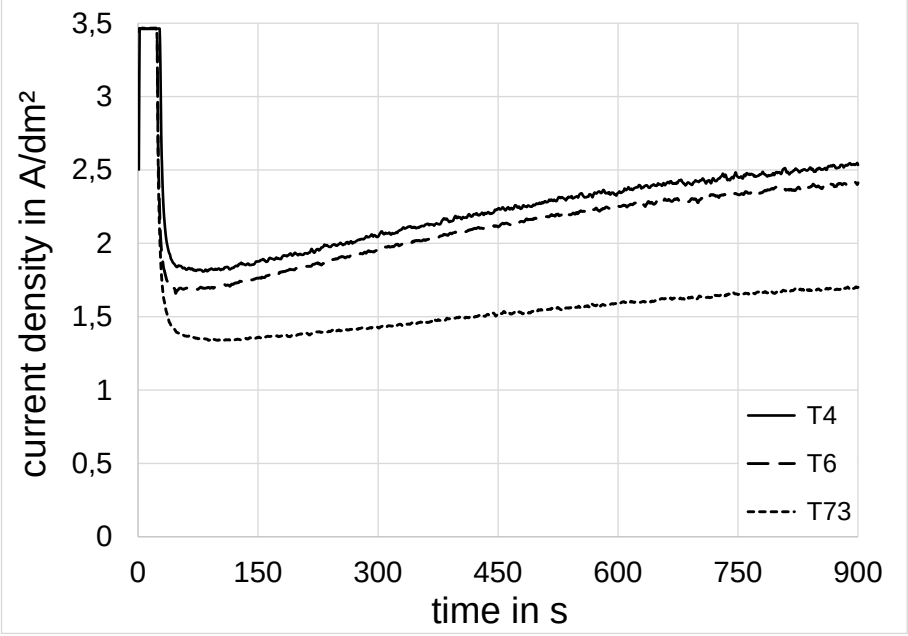

Figure 1. Profiles of the current density for the anodic oxidation of the conditions T4, T6 and T3 in 0.8 mol/l oxalic acid at a constant voltage of 60 V after the linear voltage ramp (first 30 s).

Table 1. Survey of process characteristics and coating properties.

	symbol	unit	T4	T6	T73
charge density	σ_q	As/dm²	2069±113	1899±39	1441±24
specific mass	ρ_A	mg/dm²	169.5±5.5	152.9±7.0	118.1±0.7
current efficiency	η	%	46.5±0.2	45.7±1.2	46.5±0.5
coating thickness	s	µm	8.7 ±0.2	8.1±0.5	6.0±0.1
coating porosity	p	%	43.5±2.6	45.1±5.5	42.6±0.8

3.2. Microstructure and hardness

QBSD examinations of the substrate materials were used in order to visualize the precipitations. As most of them consist of heavier elements (e.g. Zn, Fe), they appear bright in comparison to the dark Al solid solution (Alss). On the maximum magnification level, which can be realized by FE-SEM under the given conditions, no systematic differences can be observed between the conditions T4 and T6.

Figure 2 shows QBSD images of the conditions T6 (a) and T7 (b). According to [11], the microstructure of the condition T6 is characterized by spherical GP zones (less than 7.5 nm in diameter) and a small amount of the η' phase (about 10 nm in diameter). These small precipitates cannot be recognized by FE-SEM using QBSD imaging. However, as can be seen from figure 2a, also larger precipitates with up to 200 nm are present in the T6 state, both along the grain boundaries and randomly distributed within the grains. This corresponds well with the observations of Singh et al. who determined the size distribution of submicron η precipitates in EN AW-7075 T651 using FIB tomography [12]. These comparatively coarse precipitates must have developed during the processing of the sheet material prior to the T6 heat treatment (e.g. during hot rolling) and they did not dissolve completely during the solution annealing. Emani et al. observed similar η precipitates in different heat treatment conditions of EN AW-7075 and attributed their stability during solution annealing to chromium enrichment [13]. Of cause, the submicron η precipitates are also present in the T73 condition. Additionally, small bright spots can be observed in the grain interior at figure 2b. These precipitates obviously developed during the second annealing step at 160 °C which was part of the T73 treatment. Similar precipitates with up to 50 nm in diameter were identified as η' precipitates by Emani et al. after annealing at 177 °C [13]. Due to the other alloying elements and impurities, additional nano and submicron scale precipitates might be present in EN AW-7075, e.g. Mg_2Si [3]. However, because of the small differences in the atomic weight of Mg, Si and the Alss, this phase might be hardly recognizable at the QBSD images.

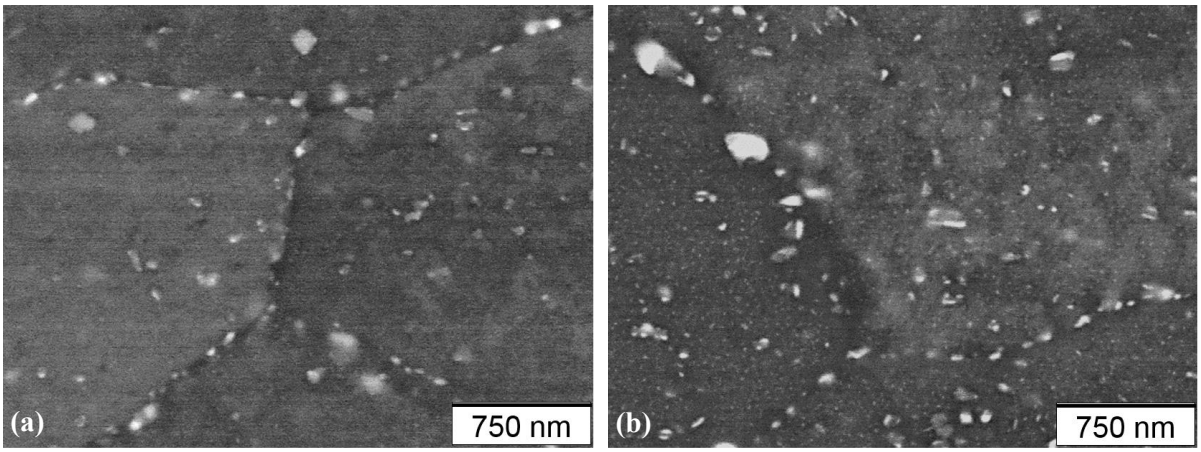

Figure 2. QBSD images of EN AW-7075 in the heat-treatment states (a) T6 showing submicron η precipitates and (b) T73 showing submicron η and nanoscale η' precipitates.

Figure 3 represents the microstructure of anodic oxide coatings on the T6 condition. The overview image (figure 3a) shows occasionally appearing oval areas (marked with (1)) within the coating exhibiting cracks perpendicular to the oxide growth direction (or parallel to the substrate coating interface, respectively). Their size and shape correspond to occasionally occurring micron scale precipitates within the substrate. The cracks indicate that the conversion of these precipitates is accompanied by a smaller volume expansion compared with the conversion of the surrounding Alss. As the cracks are not continuing through the surrounding oxide and because of their small number, these coating defects will probably not deteriorate the coating properties (e.g. hardness) significantly. Furthermore, areas with higher porosity occur at the exterior of the coatings (marked with (2)). This might be due to the chemical dissolution of the pore walls in the acidic electrolyte. The impression of this effect might be further pronounced by the final polishing of the coating cross section as more porous areas are removed faster.

Figure 3b shows the submicron and nano scale porosity of the anodic oxide coating on EN AW-7075 T6 in more detail. The characteristic pore channels are not aligned perfectly perpendicular to the substrate and parallel to each other. Some pore channels are branching and take over the area of other pore channels, while the growth of the latter stops. The competitive growth of pore channels occurs due to the faster dissolution at the bottom of some channels and therefore the faster growth of those channels [14]. Li et al. observed a highly non-conformal pore growth on high purity aluminum in 0.3 M oxalic acid at 0-5 °C and high voltages between 140 and 400 V [15]. However, some non-uniform pore growth might already occur at 60 V under the anodizing conditions described in chapter 2. Especially, the preferential dissolution of the submicron η precipitates might accelerate the progress of some pore channels and disturb the conformal pore growth. After rapid dissolution, these precipitates leave voids with similar size and shape within the oxide coating (marked by arrows in figure 3b).

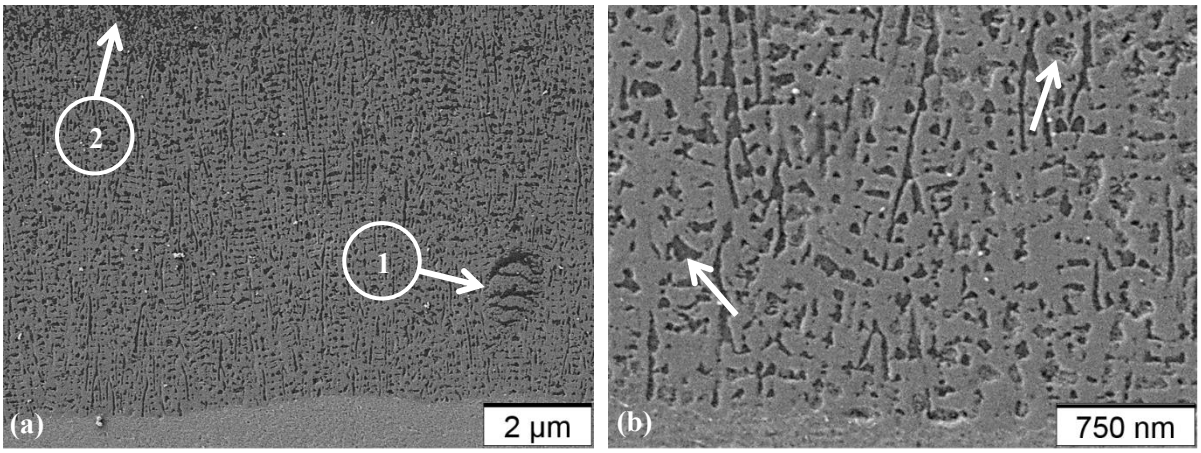

Figure 3. SE images of anodic oxide coatings on EN AW-7075 T6, (a) survey with (1) oxidized micron scale precipitate and (2) outer coating area with higher porosity, (b) detailed view in the vicinity of the substrate-coating interface showing voids due to the dissolution of submicron precipitates (marked by arrows).

As the submicron scale precipitates are also present in the T73 condition to a similar extent, the submicron scale voids are present in the oxide coatings as well (marked by arrows in figures 4a and b). Moreover, the pore channels are non-conformal for both heat treatment conditions to a similar extend. Solely the coating thickness is lower for the T73 condition due to the smaller electrical charge quantity, as already mentioned above. Possibly, the smaller η' precipitates (visible in figure 2b) give rise to the electrical resistance during anodizing leading to a decrease in the anodic current at constant voltage. However, as these small precipitates (< 50 nm) are smaller than the pore cells (~ 150 nm), they do not significantly influence the pore growth and therefore not affect the pore microstructure.

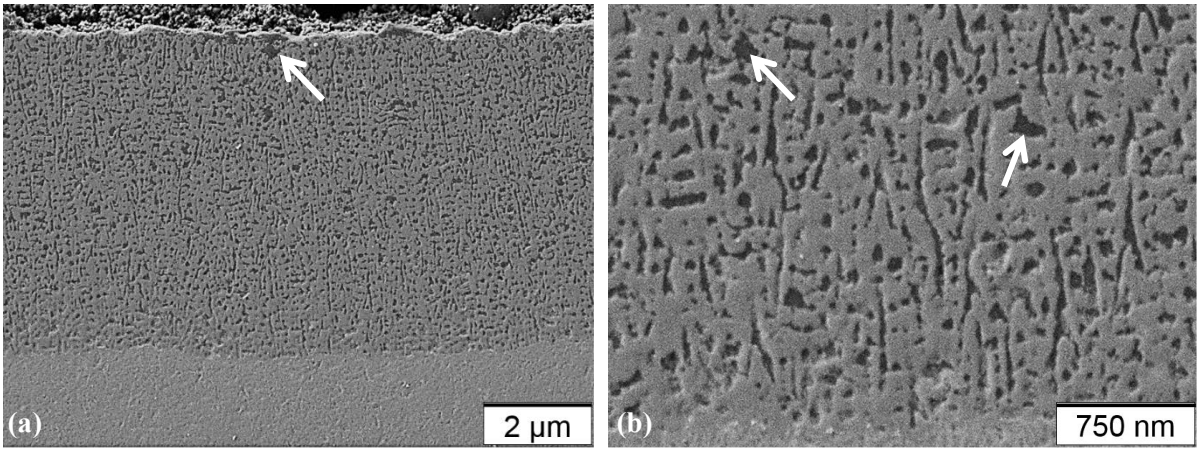

Figure 4. SE images of anodic oxide coatings on EN AW-7075 T73, (a) survey and (b) detailed view in the vicinity of the substrate-coating interface. Voids due to the dissolution of submicron precipitates are marked by arrows.

It is known from mild anodizing in sulfuric acid electrolytes at room temperature that the coating hardness significantly decreases with increasing distance from the substrate due to the chemical dissolution of the pore walls. This effect is less pronounced for the anodic oxide coatings obtained from the oxalic acid electrolyte. Figure 5 uses linear trend lines averaging about 25 data points per condition in order to display the hardness profiles more clearly. Additionally, all data points of the T4 condition are illustrated in figure 5 for giving an impression of the deviation between the trend line and the data points. It can be seen that the deviation of single data points amounts to up to 1 GPa, while most of the data points are located within a deviation of 0.5 GPa. The trend lines suggest an almost constant hardness of about 3.5 to 4 GPa (being also a typical hardness range for hard anodizing in sulfuric acid electrolytes) over a wide range of the coating thickness. Whereas for hard anodizing in sulfuric acid electrolytes, the coating hardness typically decreases more significantly within the oxide coating. This is due to the stronger chemical dissolution of the anodic alumina in sulfuric acid. As illustrated in figure 3a, areas with higher porosity are also existing in the outer part of anodic oxide coatings generated from the oxalic acid electrolyte. Therefore, a further decrease of the hardness can be expected at higher distances from the substrate-coating interface. However, due to the missing supporting effect of the surrounding material, reliable nanoindentation measurements cannot be performed in the close proximity of the outer edge. With respect to the typical deviations of the data points, the hardness levels of the different heat treatment conditions do not differ significantly. This corresponds with the fact that the anodic oxide coatings exhibit similar pore morphologies for all heat treatment conditions.

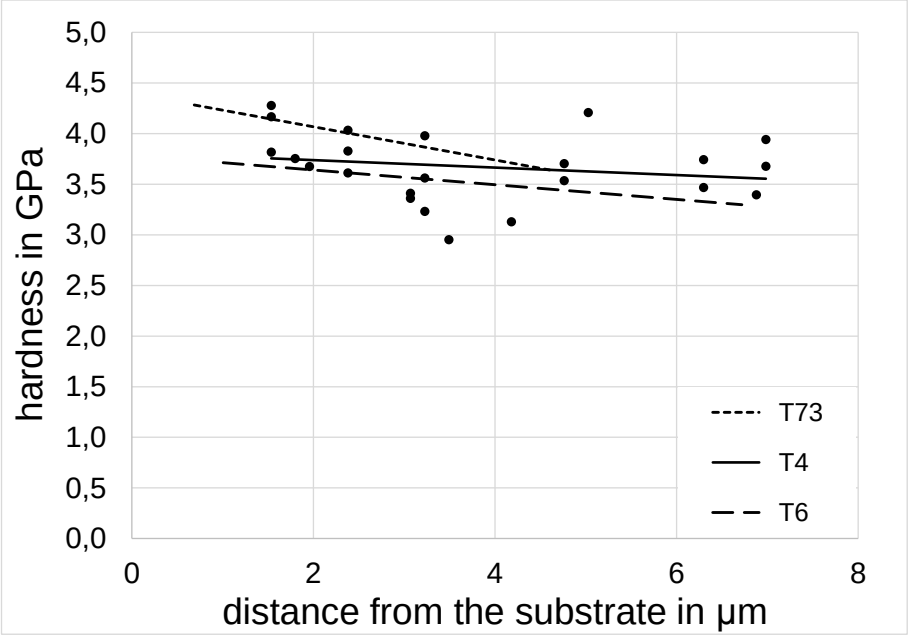

Figure 5. Linear trend lines of hardness profiles of anodic oxide coatings on heat treatment conditions T4, T6 and T73 and data points of the T4 state.

4. Conclusion

This paper describes the dependencies of coating properties (e.g. thickness, porosity, hardness) and characteristic parameters of the anodizing process in an oxalic acid electrolyte (e.g. current efficiency) on the heat treatment condition of EN AW-7075. It was found that the electrical charge density decreased by about 30 % with increasing intensity of the artificial aging from the condition T4 towards the condition T73. As coating thickness and specific mass decreased in the same proportion, it can be concluded that current efficiency and overall coating porosity were constant for all heat treatment conditions.

In order to explain the evolution of the characteristic oxide microstructure during anodizing, special attention was initially paid to the precipitates being present in the substrate materials of the industrially important conditions T6 and T73. For both conditions, a large number of submicron η precipitates were found. During anodizing, these precipitates are preferentially dissolved leading to the presence of submicron voids. Moreover, the dissolution of the precipitates disturbs the even conversion front which could be the reason for the non-conformal growth of the pore channels. The T73 condition exhibits also the presence of η’ precipitates with a size of up to 50 nm. Because of their small size, they do not influence the morphology of the pore channels significantly, however they might impede the conversion process or the charge transfer and increase the electrical resistance. Thus, the electrical current and the charge quantity are decreased. The exact role of the η’ precipitates during anodizing in oxalic acid electrolytes should be further investigated in the future.

Due to the similar pore morphologies of anodic oxide coatings on the different heat treatment conditions, similar hardness profiles were obtained by nanoindentation. The hardness level of about 3.5 to 4 GPa equals the hardness levels observed for hard anodizing in sulfuric acid electrolytes. However, unlike sulfuric acid, oxalic acid does not dissolve the pore walls in the inner part of the oxide coatings significantly. Therefore, the hardness remains almost constant over a wide range of the coating thickness.

It can be reasonably assumed that the electrolyte composition influences the conversion or dissolution of precipitates. Thus, future work should address the impact of other base electrolytes (e.g. sulphuric acid) and electrolyte additives on the anodizing behavior of different heat treatment conditions. Moreover, the conversion and dissolution kinetics of different phases depend on the applied

potential. Consequently, different electrical regimes could be applied in order to modify the morphologies of pore channels and voids with the aim of achieving desired coating properties.

5. References

[1] Wielage B, Alisch G, Lampke T and Nickel D 2008 *Key Eng. Mat.* **384** 263
[2] Sieber M, Morgenstern R, Kuhn D, Hackert-Oschätzchen M, Schubert A and Lampke T 2017 *IOP Conf. Ser.-Mat. Sci.* **181** 012044
[3] Nickel D, Dietrich D, Morgenstern R, Scharf I, Podlesak H and Lampke T 2016 *Adv. Mater. Sci. Eng.* 1374897
[4] Kuhn D, Martin A, Eckart C, Sieber M, Morgenstern R, Hackert-Oschätzchen M, Lampke T and Schubert A 2017 *IOP Conf. Ser.-Mat. Sci.* **181** 012042
[5] Zhou X, Habazaki H, Shimizu K, Skeldon P, Thompson GE and Wood GC 1996 *Corros. Sci.* **38** 1563
[6] Thompson GE, Habazaki H, Shimizu K, Sakairi M, Skeldon P, Zhou X and Wood GC 1999 *Aircr. Eng. Aerosp. Tec.* **71** 228
[7] Morgenstern R, Dietrich D, Sieber M and Lampke T 2017 *IOP Conf. Ser.-Mat. Sci.* **181** 012043
[8] Mukhopadhyay AK 1998 *Metall. Mater. Trans. A* **29A** 979
[9] Veys-Renaux D, Chahbouna N and Rocca E 2016 *Elektrochim. Acta* **211** 1056
[10] Li J, Peng Z, Li C, Jia Z, Chen W and Zheng Z 2008 *Trans. Nonferrous Met. Soc. China* **18** 755
[11] Delasi R and Adler PN 1977 *Metall. Trans. A* **8A** 1177
[12] Singh SS, Loza JJ, Merkle AP and Chawla N 2016 *Mater. Charact.* **118** 102
[13] Emani SV, Benedyk J, Nash P and Chen D 2009 *J. Mater. Sci.* **44** 6384
[14] Chen S, Ling Z, Hu X, Yang H and Li Y 2010 *J. Mater. Chem.* **20** 1794
[15] Li Y, Ling Z, Hu X, Liu Y and Chang Y 2011 *J. Mater. Chem.* **21** 9661

Acknowledgments
The authors gratefully acknowledge funding of this work by the German Research Foundation (Deutsche Forschungsgemeinschaft, DFG, project LA1274/40-1). The support by Dagobert Spieler, Elke Benedix, Steffen Clauß, Christel Gläser and Paul Clauß (all from the Institute of Materials Science and Engineering) is gratefully acknowledged.